

Article

# The Carbon Additive Effect on Electrochemical Performance of $\text{LiFe}_{0.5}\text{Mn}_{0.5}\text{PO}_4/\text{C}$ Composites by a Simple Solid-State Method for Lithium Ion Batteries

Chun-Chen Yang <sup>1,2,\*</sup>, Yen-Wei Hung <sup>1</sup> and Shingjiang Jessie Lue <sup>3</sup>

<sup>1</sup> Department of Chemical Engineering, Ming Chi University of Technology, New Taipei City 243, Taiwan; mi-nered@hotmail.com

<sup>2</sup> Battery Research Center of Green Energy, Ming Chi University of Technology, New Taipei City 243, Taiwan

<sup>3</sup> Department of Chemical and Materials Engineering and Green Technology Research Center, Chang Gung University, Kwei-shan, Taoyuan 333, Taiwan; jessie@mail.cgu.edu.tw

\* Correspondence: ccyang@mail.mcut.edu.tw; Tel.: +886-2-2908-9899

Academic Editor: Maciej Swierczynski

Received: 28 April 2016; Accepted: 7 June 2016; Published: 15 June 2016

**Abstract:** This work reported a solid-state method to prepare  $\text{LiFe}_{0.5}\text{Mn}_{0.5}\text{PO}_4/\text{C}$  (LFMP/C) composite cathode materials by using  $\text{LiH}_2\text{PO}_4$ ,  $\text{MnO}_2$ ,  $\text{Fe}_2\text{O}_3$ , citric acid ( $\text{C}_6\text{H}_8\text{O}_7$ ), and sucrose ( $\text{C}_{12}\text{H}_{22}\text{O}_{11}$ ). The citric acid was used as a complex agent and  $\text{C}_{12}\text{H}_{22}\text{O}_{11}$  was used as a carbon source. Two novel hollow carbon sphere (HCS) and nanoporous graphene (NP-GNS) additives were added into the LFMP/C composite to enhance electrochemical performance. The HCS and NP-GNS were prepared via a simple hydrothermal process. The characteristic properties of the composite cathode materials were examined by micro-Raman spectroscopy, X-ray diffraction (XRD), scanning electron microscopy (SEM), elemental analysis (EA), and alternating current (AC) impedance methods. The coin cell was used to investigate the electrochemical performance at various rates. It was found that the specific discharge capacities of LFMP/C + 2% NP-GNS + 2% HCS composite cathode materials were 161.18, 154.71, 148.82, and 120.00  $\text{mAh} \cdot \text{g}^{-1}$  at 0.1C, 0.2C, 1C, and 10C rates, respectively. Moreover, they all showed the coulombic efficiency *ca.* 97%–98%. The advantage of the one-pot solid-state method can be easily scaled up for mass-production, as compared with the sol-gel method or hydrothermal method. Apparently, the LFMP/C composite with HCS and NP-GNS conductors can be a good candidate for high-power Li-ion battery applications.

**Keywords:**  $\text{LiFe}_{0.5}\text{Mn}_{0.5}\text{PO}_4$  (LFMP);  $\text{Fe}_2\text{O}_3$ ;  $\text{MnO}_2$ ; specific capacity; cathode materials; solid-state method

## 1. Introduction

Li-ion batteries are appropriate for use in cell phones, laptop computers, digital cameras, renewable energy storage, and smart grid applications because of their relatively high energy density, low cost, and high rate capabilities. Li-ion batteries used in hybrid-electric vehicle or electric vehicle applications must be charged and discharged rapidly; therefore, the electrodes must perform at a high rate and maintain high discharge capacity and reliable cycle-life stability. Compared with the  $\text{LiFePO}_4$  cathode material [1], the  $\text{LiMnPO}_4$  cathode material exhibits a higher working potential at 4.1 V (*versus*  $\text{Li}/\text{Li}^+$ ) and is compatible with conventional liquid carbonate-based electrolytes. The energy density of the  $\text{LiMnPO}_4$  ( $697 \text{ Wh} \cdot \text{kg}^{-1}$ ) [2] is higher than that of the  $\text{LiFePO}_4$  ( $586 \text{ Wh} \cdot \text{kg}^{-1}$ ); however, the electrical conductivity of the  $\text{LiMnPO}_4$  material (less than  $10^{-10} \text{ S} \cdot \text{cm}^{-1}$ ) is much lower than that of the  $\text{LiFePO}_4$  material (at  $1.8 \times 10^{-8} \text{ S} \cdot \text{cm}^{-1}$ ). The electrochemical performance can be improved by coating the samples' surface with carbon, or by doping with Fe atoms or nano-sized cathode materials. Olive phosphate materials combined with mixed transition-metal ions, such as

$\text{LiFe}_{1-x}\text{Mn}_x\text{PO}_4/\text{C}$ , have recently attracted considerable attention [3–14]. Zou *et al.* [15] prepared  $\text{LiFe}_{0.2}\text{Mn}_{0.8}\text{PO}_4/\text{C}$  cathode materials by a solid-state method and sucrose used as the carbon source. The as-prepared cathode materials achieved capacities of  $150 \text{ mAh g}^{-1}$  and  $110 \text{ mAh g}^{-1}$  at  $1/20\text{C}$  and  $1\text{C}$ , respectively. Liu *et al.* [16] recently synthesized a  $\text{LiMn}_{1-x}\text{Fe}_x\text{PO}_4/\text{C}$  ( $x = 0.1, 0.2, 0.3$ ) cathode material by a ball-milling process with  $\text{MnPO}_4 \cdot \text{H}_2\text{O}$  precursors,  $\text{LiOH}$ ,  $\text{NH}_4\text{H}_2\text{PO}_4$ , and 30 wt% glucose. The as-prepared  $\text{LiMn}_{0.7}\text{Fe}_{0.3}\text{PO}_4/\text{C}$  cathode material had a capacity of  $140 \text{ mAh g}^{-1}$  and high rate performance. Mi *et al.* [17] prepared mesoporous  $\text{LiFe}_{0.6}\text{Mn}_{0.4}\text{PO}_4/\text{C}$  materials—comprising of different amounts of multi-wall carbon nanotubes (MWCNTs) by using a two-step carbon coating and spray drying process. The  $\text{LiFe}_{0.6}\text{Mn}_{0.4}\text{PO}_4/\text{C}$  materials with 2 wt% MWCNTs showed excellent performance by delivering a discharge capacity of  $163.3 \text{ mAh g}^{-1}$  at  $0.1\text{C}$  and yielding an ultra-high rate capacity of  $64.23 \text{ mAh g}^{-1}$  at  $50\text{C}$ . Hu *et al.* [18] prepared Fe-doped  $\text{LiMn}_{1-x}\text{Fe}_x\text{PO}_4$  ( $x = 0.5$ ) nanomaterials by using a solvothermal method.  $\text{LiMn}_{0.5}\text{Fe}_{0.5}\text{PO}_4$  notably delivered a 100% capacity retention with a discharge capacity of  $147 \text{ mAh g}^{-1}$  at  $1\text{C}$  rate. Zhong *et al.* [19] most recently synthesized a carbon-coated  $\text{LiFe}_{0.5}\text{Mn}_{0.5}\text{PO}_4/\text{C}$  (LFMP/C) material by a rheological phase reaction method with stearic acid as the carbon source (*i.e.*, a solid-state method). The LFMP/C material exhibited the highest electrochemical performance compared with the  $\text{LiMn}_{0.2}\text{Fe}_{0.8}\text{PO}_4/\text{C}$  and  $\text{LiMn}_{0.8}\text{Fe}_{0.2}\text{PO}_4/\text{C}$  materials. The LFMP/C material delivered discharge capacities of 138, 99, 80, 72, 67, and  $55 \text{ mAh g}^{-1}$  at  $0.1\text{C}$ ,  $1\text{C}$ ,  $5\text{C}$ ,  $10\text{C}$ ,  $15\text{C}$ , and  $20\text{C}$  rates, respectively. The LFMP/C material achieved long and stable cycling performance with a capacity of  $103 \text{ mAh g}^{-1}$  at  $1\text{C}$  rate during a 100-cycle test.

In this work, nanostructured carbon materials show a variety of fascinating and admirable properties for Li-ion batteries, such as high surface area, low diffusion distance, and high electron and ionic conductivity [20,21]. Therefore, nano-sized carbon materials show extremely promising to improve the discharge capacity, the power capability, and the long cycling stability. We studied the carbon conductor effect on performances of LFMP/C composite. Both hollow carbon sphere (HCS) and nanoporous graphene (NP-GNS) were synthesized by a hydrothermal process. The characteristic properties of the LFMP/C composite cathode materials were examined by micro-Raman spectroscopy, X-ray diffraction (XRD), scanning electron microscopy (SEM), elemental analysis (EA), and alternating current (AC) impedance method.

## 2. Experimental

### 2.1. Preparation of Hollow Carbon Sphere and Nanoporous Graphene Carbon Conductors

The HCS was also synthesized by a simple, one-pot, green, hydrothermal process. In a typical procedure [22], 40 g glucose (Aldrich, St. Louis, MO, USA) and 4 g sodium dodecyl sulfate (SDS, Aldrich) were first dissolved into in 460 mL distilled water. Then, the resultant solution was stirred for three days at  $50^\circ\text{C}$ . The obtained mixture solution was transferred into a Teflon-lined autoclave of 600 mL capacity with a stainless steel shell, followed by a hydrothermal treatment at  $190^\circ\text{C}$  for 10 h. After that, the autoclave was allowed to reach room temperature. The as-prepared carbon sphere materials was filtered and washed with distilled water and ethanol several times, and then dried at  $80^\circ\text{C}$  for overnight. The HCS materials were obtained by sintering the as-prepared powders at  $900^\circ\text{C}$  for 4 h in  $\text{N}_2$  atmosphere.

The nanoporous graphene oxide (GO) was fabricated by a solvothermal process [23]. Both the as-prepared GO and ferrocene were used as the precursors. The concentration of GO solution was around  $4 \text{ mg mL}^{-1}$ . The ratio of GO to ferrocene was kept at 1:20. The solvothermal process was carried out at  $180^\circ\text{C}$  for 10 h. The mixture solid product was separated through filtration, washed with ethanol for several times to remove the residual ferrocene, and then dried. The ferrocene/GO mixed composite was annealed at  $800^\circ\text{C}$  for 4 h in a 95% Ar/5%  $\text{H}_2$  atmosphere; at the same time, the ferrocene was decomposed into iron/Austenite nanosphere. The iron/Austenite nanosphere was further removed with 12 M HCl solution, then nano-porous graphene sheet was obtained through

filtration and annealed in Ar at 800 °C for 1 h. The NP-GNS was generated through a simple thermal reduction process.

## 2.2. Preparation of $\text{LiFe}_{0.5}\text{Mn}_{0.5}\text{PO}_4/\text{C}$ Materials

The LFMP/C cathode materials were prepared using a wet-balled method. Appropriate amounts of  $\text{LiH}_2\text{PO}_4$ ,  $\text{Fe}_2\text{O}_3$ ,  $\text{MnO}_2$ , carbon black (BP2000), sucrose, and citric acid (Aldrich, 99%) as starting materials were dissolved in acetone. The molar ratio of Li:Fe:Mn:P was 1:0.5:0.5:1. Approximately 10 wt% sucrose and 5 wt% citric acid were used as the carbon source and complex agent, respectively. The sucrose and citric acid were mixed with the acetone and starting raw materials and then wet ball-milled (Planetary Ball-Milling Apparatus, ball-to-powder weight ratio = 10:1, Primum Line, Fritsch, Idar-Oberstein, Germany) at 400 rpm for approximately 10–15 h. The ball-milling process was performed in an inert atmosphere that was controlled to avoid the  $\text{Fe}^{2+}$  and  $\text{Mn}^{2+}$  species from oxidation. The ball-milled mixture was dried and subsequently heated at 650, 675, and 700 °C for 15 h in an argon atmosphere. The carbon content was approximately 5%–9%. The LFMP/C + 2% graphene (denoted as NP-GNS) + 2% carbon sphere (denoted as CS) composites were prepared by adding nano-sized graphene (16 nm thickness,  $50 \text{ m}^2 \cdot \text{g}^{-1}$ ) and carbon sphere (prepared by a hydrothermal process). The obtained LFMP/C composite precursor was further calcined at 650, 675, and 700 °C for 15 h in an argon atmosphere. The residual carbon content was approximately 5%–9%.

## 2.3. Material Characterization

The crystal structures of the as-prepared LFMP/C samples were examined using an XRD spectrometer (D2 Phaser, Bruker, Karlsruhe, Germany). The surface morphology and the residual carbon morphology were examined using SEM (Hitachi, Toyo, Chiba, Japan) and high-resolution transmission electron microscopy (HR-TEM, JEOL 2010F, Toyo), respectively. The micro-Raman spectra were recorded using a confocal micro-Renishaw fitted with a 632 nm He–Ne excitation laser (Renishaw inVia, London, UK). The residual carbon content in the sample was examined using an elemental analyzer (FLASH 2000, Thermo Fisher Scientific, Waltham, MA, USA).

## 2.4. Electrochemical Performance of $\text{LiFe}_{0.5}\text{Mn}_{0.5}\text{PO}_4/\text{C}$

The electrochemical performances of the LFMP/Li and LFMP/C + 2% NP-GNS + 2% HCS half-cells were measured using a two-electrode system (*i.e.*, CR-2032 coin cells assembled in an Ar-filled glove box). The LFMP/C composite electrodes were prepared by mixing active LFMP/C materials with Super P and poly(vinyl fluoride) (PVDF) binder at a weight ratio of 80:10:10 [24]. The resulting sample was coated on an Al foil (Aldrich) and dried in a vacuum oven at 80 °C for 12 h. Li foils (Aldrich) were used as the counter and reference electrodes, and a microporous polyethylene (PE) film (Celgard 2400, Charlotte, NC, USA) was used as the separator. The active material loading on Al current collector is around  $2\text{--}3 \text{ mg} \cdot \text{cm}^{-2}$ , and the thickness of the dried LFMP/C electrode is about 30 µm. The total thickness of the electrode is 50 µm; the Al current collector is 20 µm. The electrolyte was 1 M of  $\text{LiPF}_6$  in a mixture of EC and DEC (1:1 in v/v, Merck, Kenilworth, NJ, USA). The LFMP/Li half-cells were charged at a constant current (CC) and a potential range of 2.0–4.5 V (*versus*  $\text{Li}/\text{Li}^+$ ) at 0.1C-rate, using a battery tester (Arbin BT2000, College Station, TX, USA). However, the LFMP/Li cells were charged using a CC–CV protocol, and discharged using a CC profile, at a potential range of 2.0–4.5 V (*versus*  $\text{Li}/\text{Li}^+$ ) at various C-rates (*i.e.*, 0.2–10C-rates) by using a battery tester (Arbin BT2000). The second CV charge step of 4.5 V was terminated when the charge current was less than 0.1C. The AC spectra of LFMP/Li half-cells were measured at room temperature an Autolab PGSTAT-30 electrochemical system with GPES 4.8 Package Software (Eco Chemie, B.V., Utrecht, The Netherlands).

## 3. Results and Discussion

Figure 1a shows the typical SEM image of HCS via a hydrothermal carbonation of glucose. The size of HCS is around 1–2 µm; they have hollow and semi-hollow structure. Figure 1b shows the XRD pattern of the HCS sample. Two broad peaks are located at  $24^\circ$  and  $43^\circ$  that correspond to the

(002) and (101) planes, indicating the graphitic state of HCS sample. Figure 1c shows the SEM image of NP-GNS sample. They show a highly curved morphology with a nanoporous structure.

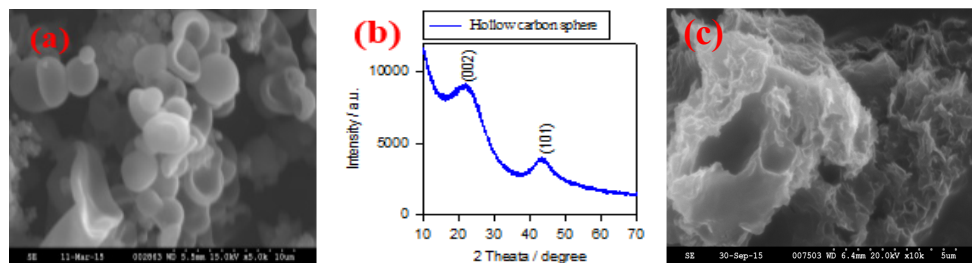


**Figure 1.** (a) Scanning electron microscopy (SEM) image for hollow carbon sphere (HCS); (b) X-ray diffraction (XRD) pattern for HCS; and (c) SEM image for nanoporous graphene (NP-GNS) at 3k $\times$ .

Figure 2 shows the XRD patterns of the LFMP/C and LFMP/C + 2% NP-GNS + 2% HCS samples prepared using the wet ball-milling method at 650–700 °C. All of the Bragg diffraction peaks of the compounds were well-indexed based on a single-phase olivine-type structure indexed with the orthorhombic *Pnma* space group. No impurity peaks, such as Li<sub>3</sub>PO<sub>4</sub> and Mn<sub>2</sub>P<sub>2</sub>O<sub>7</sub> phases, were found. By comparison, the lattice parameters of the LFP/C, LFMP/C, and SP-LFMP/C composite samples are listed in Table 1. The carbon peaks cannot be observed because of the small amount of the residual carbon content (C% *ca.* 5%–9%) with amorphous configuration. Fe<sup>2+</sup> and Mn<sup>2+</sup> ions were located at the tetrahedral 4c sites in LiFe<sub>1-y</sub>Mn<sub>y</sub>PO<sub>4</sub> ( $y = 0.5$ ). The Mn<sup>2+</sup> ion (with an ionic radius of 0.97 Å) has a larger ionic size than the Fe<sup>2+</sup> ion (with an ionic radius of 0.92 Å). It was found that the LFMP/C composite materials increased as the Mn<sup>2+</sup>-doping concentration increased. In addition, the unit cell volume of the LFMP/C composite materials increased linearly with the Mn<sup>2+</sup>-substitution. As shown in Figure 1, the peaks of the LFMP/C sample (*i.e.*, 301, 121, and 410) shifted to the lower angle direction compared with those of the LFP/C sample [20]. The primary crystal sizes of the LFMP/C and the LFMP/C + 2% NP-GNS + 2% HCS composite materials estimated using Scherrer's equation were *ca.* 50–65 nm. The content of residual carbon is studied by elemental analysis (EA) in the composites lists in Table 2. The residual carbon content of the LFMP/C materials with 5 wt% sucrose, 20 wt% citric acid, and 5 wt% BP2000 at different sintering temperatures are around 7.4%–4.8%; in contrast, the residual carbon of the LFMP/C + 2% NP-GNS + 2% HCS composite materials with adding extra 2% NP-GNS + 2 wt% HCS carbon conductor is around 9.31%. Clearly, the residual carbon content decreases when the sintering temperature was increased. It was also found that the electrical conductivity of the LFMP/C + 2% NP-GNS + 2% HCS composite materials can be improved to *ca.* 10<sup>-3</sup> S·cm<sup>-1</sup>.

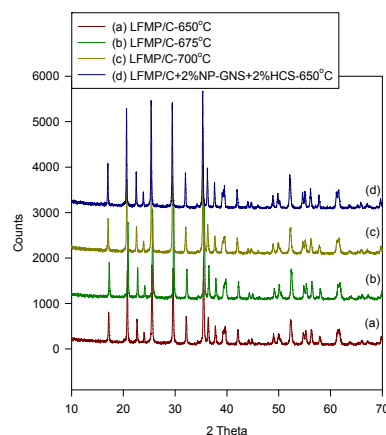


**Figure 2.** XRD patterns of all LiFe<sub>0.5</sub>Mn<sub>0.5</sub>PO<sub>4</sub>/C (LFMP/C) sample.

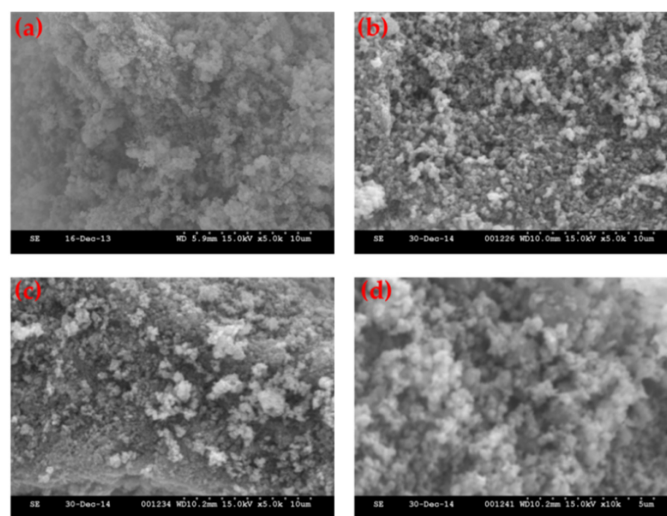
**Table 1.** The lattice parameters of all LFMP/C samples from XRD analysis.

Sample	LFMP/C-650	LFMP/C + 2% NP-GNS + 2% HCS-650	LFMP/C-675	LFMP/C-700
<i>a</i> (nm)	0.47216	0.47138	0.47184	0.47177
<i>b</i> (nm)	1.03957	1.03826	1.03926	1.03904
<i>c</i> (nm)	0.60575	0.60499	0.60545	0.60542
<i>V</i> (nm <sup>3</sup> )	0.29733	0.29609	0.29690	0.29686

**Table 2.** The residual carbon contents of all LFMP/C samples by elemental analysis (EA).

Sample	Sample#1/mg	Sample#2/mg	C#1/wt%	C#2/wt%	C <sub>avg</sub> /wt%
LFMP/C-650	1.88	2.33	7.34	7.40	7.37
LFMP/C-675	1.97	2.4	5.19	5.31	5.25
LFMP/C-700	1.71	1.94	4.76	4.85	4.81
LFMP/C + 2% NP-GNS + 2% HCS-650	2.11	1.88	9.31	9.31	9.31

Figure 3 shows the SEM images of the LFMP/C-650, LFMP/C-670, LFMP/C-700, and LFMP/C + 2% NP-GNS + 2% HCS-650 composites prepared via the wet ball-milled method. The secondary particle sizes of the LFMP/C composite ranged from 2  $\mu\text{m}$  to 10  $\mu\text{m}$  with a spherical morphology. The surface is highly porous with a macro/nano three-dimensional (3D) hierarchical structure. Figure 3d also shows the SEM images of the LFMP/C + 2% NP-GNS + 2% HCS-650 composites. The LFMP/C + 2% NP-GNS + 2% HCS-650 composite with two conductive carbons added shows a good conductive network because of the uniform coverage of the carbon on the surface of LFMP/C material. In other words, the double carbons greatly improved the coating uniformity on the LFMP/C composite material (see later for transmission electron microscopy (TEM) and micro-Raman results). More importantly, the LFMP/C composite showed slightly smaller particles size around 50 nm; it is due to the high content of carbon being added (C% = 9%). It is well accepted that the carbon precursors can inhibit the LFMP crystalline growth [24]. Therefore, it was well accepted that the smaller particle size of LFPM/C will have much shorter Li<sup>+</sup> ion diffusion length. It will greatly improve the electrochemical performance, in particular at high rate. Figure 4 shows the HR-TEM images of the LFMP/C and LFMP/C + 2% NP-GNS + 2% HCS samples sintered at 650–700 °C. It was found that a uniform carbon coating on LFMP/C samples sintered at temperatures of 650, 675, and 700 °C with the thickness of approximately 10, 3, and 2 nm, respectively, was observed. In contrast, Figure 4h presents the TEM image for the LFMP/C + 2% NP-GNS + 2% HCS composite sintered at 650 °C. It was shown the much thick carbon layer is around 4.7 nm.

**Figure 3.** SEM images of LFMP/C sample in 5 k $\times$ : (a) LFMP/C-650; (b) LFMP/C-675; (c) LFMP/C-700; and (d) LFMP/C + 2% NP-GNS + 2% HCS-650.

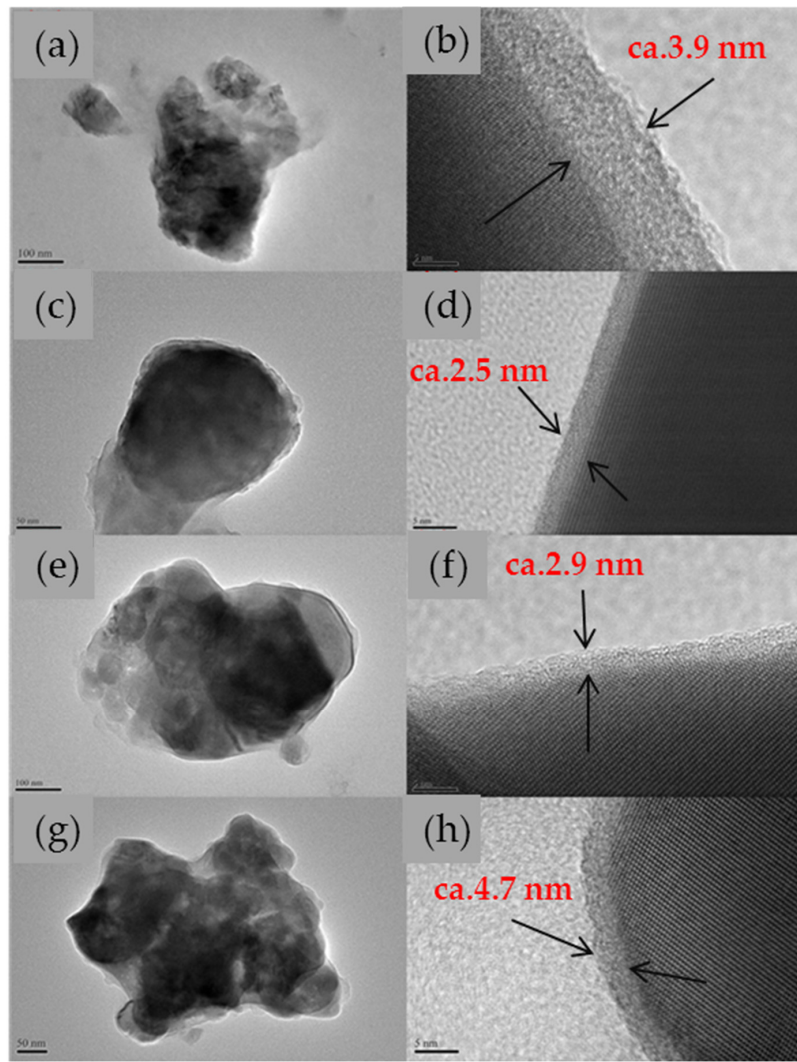


**Figure 4.** High-resolution transmission electron microscopy (HR-TEM) images of LFMP/C sample: (a,b) LFMP/C-650; (c,d) LFMP/C-675; (e,f) LFMP/C-700; and (g,h) LFMP/C + 2% NP-GNS + 2% HCS-650.

Figure 5 shows the micro-Raman spectra of the LFMP/C samples and the LFMP/C + 2% NP-GNS + 2% HCS composite, indicating three major Raman vibration peaks at  $951\text{ cm}^{-1}$ ,  $1328\text{ cm}^{-1}$ , and  $1585\text{ cm}^{-1}$ . Several Raman peaks at approximately between  $947\text{--}950\text{ cm}^{-1}$  and  $596\text{--}446\text{ cm}^{-1}$  were identified as the vibration of the P–O bond, and the peak located at  $638\text{ cm}^{-1}$  was identified as the vibration of the  $\text{FeO}_x$  groups. Two Raman peaks of the LFMP/C samples and the LFMP/C + 2% NP-GNS + 2% HCS composite were located at approximately  $1328\text{ cm}^{-1}$  and  $1585\text{ cm}^{-1}$ ; these peaks were attributed to the residual carbon source. Raman peaks at  $1326\text{ cm}^{-1}$  (D-band) and  $1588\text{ cm}^{-1}$  (G-band) was observed in the LFMP/C + 2% NP-GNS + 2% HCS composite. Broadening the D ( $A_{1g}$  symmetry) and G ( $E_{2g}$  symmetry) bands with a strong D-band indicated a localized in-plane  $\text{sp}^2$  graphitic crystal domain and a disordered  $\text{sp}^3$  amorphous carbon, respectively. The intensity ratio of the D-band to the G-band (*i.e.*,  $R = I_D/I_G$ ) was used to estimate the carbon quality of the LFMP/C samples. The  $R$ -value of the LFMP/C samples at various sintered temperatures of  $650\text{--}700\text{ }^\circ\text{C}$  ( $R = 1.11\text{--}1.12$ ) was slightly lower than that of the LFMP/C + 2% NP-GNS + 2% HCS composite ( $R = 1.15$ ). The discharge capacities and rate capabilities of the LFMP/C samples are strongly related to the intensity ratio of the D- and G-bands [22–24]. Table 3 shows the  $R$  values of all LFMP/C samples by micro-Raman analysis in detail.

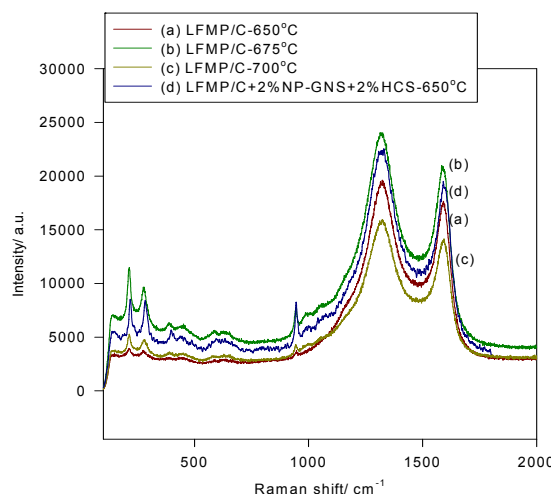


**Figure 5.** Micro-Raman curve of all LFMP/C samples.

**Table 3.** Micro-Raman spectroscopic analysis of LFMP/C samples.

Samples	$I_D$	$I_G$	$\text{PO}_4^{3-}$	$R = I_D/I_G$	$(I_D + I_G)/\text{PO}_4^{3-}$
LFMP/C-650	19,627	17,656	3761	1.112	9.91
LFMP/C-675	24,021	20,940	7773	1.147	5.78
LFMP/C-700	15,962	14,166	4286	1.124	7.03
LFMP/C + 2% NP-GNS + 2% HCS-650	22,399	19,508	8270	1.148	5.07

Figure 6 shows the initial charge/discharge profiles of three LFMP/C samples, *i.e.*, LFMP-650, LFMP/C-675, and LFMP/C-700, and the LFMP/C + 2% NP-GNS + 2% HCS composite at 0.1C rate and 25 °C, indicating that the LFMP/Li half-cell displayed two flat discharge plateaus at *ca.* 4.00–4.03 V and *ca.* 3.50–3.55 V (*versus* Li/Li<sup>+</sup>), respectively, associated with two Mn<sup>3+</sup>/Mn<sup>2+</sup> and Fe<sup>3+</sup>/Fe<sup>2+</sup> redox pairs. The LFMP/C, based on a wet ball-milled method, half-cells based on the as-synthesized materials yielded an initial discharge capacity of 148, 139, and 144 mAh·g<sup>-1</sup> at 0.1C, respectively. By contrast, as shown in Figure 6, the LFMP/C + 2% NP-GNS + 2% HCS composite showed an initial discharge capacity of around 161.2 mAh·g<sup>-1</sup> at 0.1C, indicating that it is superior in performance to the LFMP/C composite with a suitable amount of carbon additives, *ca.* 4 wt% here. Figure 6 reveals the typical charge/discharge curves of the LFMP/C + 2% NP-GNS + 2% HCS composite at various discharge rates, *i.e.*, at 0.2–10C.

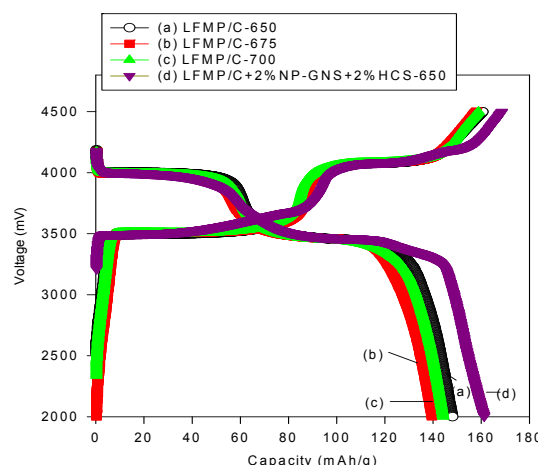


**Figure 6.** The initial sample charge/discharge curves of LFMP/C samples at 0.1C/0.1C at 25 °C.

The LFMP/C + 2% NP-GNS + 2% HCS composite exhibited discharge capacities of 154.7, 150.3, 148.8, 136.7, 130.3, and 120.0  $\text{mAh} \cdot \text{g}^{-1}$  at charge/discharge rates of 0.2C/0.2C, 0.2C/0.5C, 0.2C/1C, 0.2C/3C, 0.2C/5C, and 0.2C/10C, respectively. These results indicate that the LFMP/C + 2% NP-GNS + 2% HCS composite exhibited excellent high-rate capability and reliable cycle-life stability. In a previous study [17], the discharge capacities of a  $\text{LiFe}_{0.6}\text{Mn}_{0.4}\text{PO}_4/\text{C}$  sample containing 2 wt% MWCNTs and prepared using a spray drying method—were *ca.* 163.3  $\text{mAh} \cdot \text{g}^{-1}$  and 148.7  $\text{mAh} \cdot \text{g}^{-1}$  at 0.1C-rate and 1C-rate, respectively. These results are comparable with our results, which are *ca.* 161  $\text{mAh} \cdot \text{g}^{-1}$  and 149  $\text{mAh} \cdot \text{g}^{-1}$  at 0.1C and 1C rate, respectively. However, in Zhong *et al.* [19], the discharge capacities of a LFMP/C material prepared by using a rheological phase method—were 138  $\text{mAh} \cdot \text{g}^{-1}$  and 100  $\text{mAh} \cdot \text{g}^{-1}$  at 0.1 and 1C-rate, respectively; these findings show that our sample results are clearly superior to their results.

Figure 7 presents a comparison of the rate capability performance of the LFMP/Li half-cell based on the LFMP/C samples (without carbon additives) and the LFMP/C + 2% NP-GNS + 2% HCS composite comprised of extra 2 wt% NP-GNS + 2 wt% HCS carbon conductors, at 0.2–10C rates. We observed that the LFMP/C + 2% NP-GNS + 2% HCS composite exhibited higher rate performance than that of the LFMP/C sample. As shown in Figure 8, the discharge specific capacities of the LFMP/C + 2% NP-GNS + 2% HCS composite sintered at 650 °C decreased from 154  $\text{mAh} \cdot \text{g}^{-1}$  to 120  $\text{mAh} \cdot \text{g}^{-1}$  as the discharge rate was increased from 0.2C to 10C. By contrast, the discharge-specific capacities of the LFMP/C samples sintered at the same temperature of 650 °C decreased from 141  $\text{mAh} \cdot \text{g}^{-1}$  to 113  $\text{mAh} \cdot \text{g}^{-1}$ . We observed that the rate capability performance of the LFMP/C + 2% NP-GNS + 2% HCS composite with a two-type of carbon conductors, namely, two-dimensional (2D)-graphene and 3D carbon sphere, is greatly improved, as compared to the LFMP/C material without any carbon conductor.

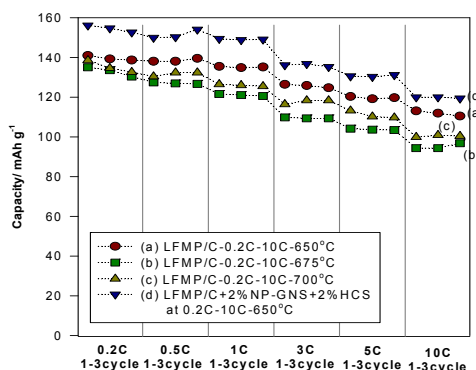


**Figure 7.** The rate capability curves of all LFMP/C samples at 0.2–10C.

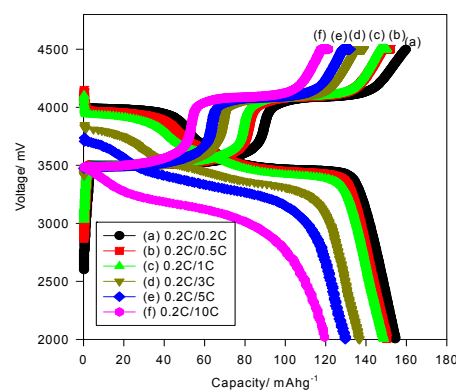


**Figure 8.** The charge/discharge curves of the LFMP/C + 2% NP-GNS + 2% HCS composite sintered at 650 °C at 0.2–10C rates.

Figure 9A shows the cycle-life performance of the LFMP/C-650, LFMP/C-675, and LFMP/C-700 samples, and the LFMP/C + 2% NP-GNS + 2% HCS composite at charge/discharge rate of 0.1C/0.1C for 30 cycles for comparison. It was found that the discharge capacity of the LFMP/C-650 sample was maintained at  $141\text{--}139\text{ mAh}\cdot\text{g}^{-1}$  at 0.1C-rate during the 30 cycling test, and the average discharge capacity was approximately  $141\text{ mAh}\cdot\text{g}^{-1}$ , demonstrating excellent cycle stability with no apparent capacity after the 30-cycle test. We observed that the average current efficiency of the LFMP/C-650 sample at 0.1C was approximately 99.32% during the 30-cycle test. Moreover, the discharge capacity of the LFMP/C-675 sample was maintained at  $145\text{--}137\text{ mAh}\cdot\text{g}^{-1}$  at 0.1C-rate during the 30 cycles. The average discharge capacity was approximately  $137\text{ mAh}\cdot\text{g}^{-1}$  with a fading rate of  $-0.57\%/\text{cycle}$  at 0.1C rate during the cycling test. In addition, it was found that the average coulombic efficiency of the LFMP/C-675 sample at 0.1C was approximately 99.3% during the 30-cycle test. Furthermore, the discharge capacity of the LFMP/C-700 sample was maintained at  $148\text{--}139\text{ mAh}\cdot\text{g}^{-1}$  at 0.1C-rate during the 30 cycles. The average discharge capacity was approximately  $140\text{ mAh}\cdot\text{g}^{-1}$  with a fading rate of  $-0.63\%/\text{cycle}$  at 0.1C rate during the cycling test. In addition, it was revealed that the average current efficiency of the LFMP/C-700 sample at 0.1C was approximately 99.3% during the 30-cycle test.

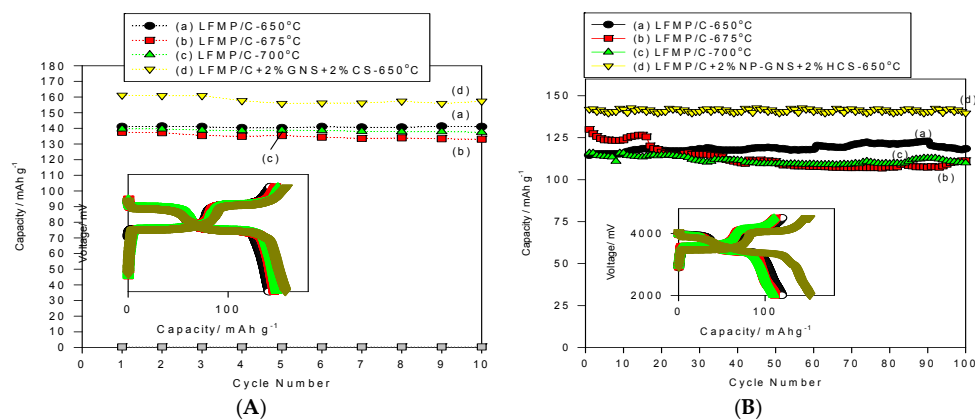


**Figure 9.** The cycle-life performance of all LFMP/C samples at: (A) 0.1C/0.1C rate; and (B) 1C/1C rate.

As expected, the discharge capacity of the LFMP/C + 2% NP-GNS + 2% HCS composite was achieved at  $161\text{--}155\text{ mAh}\cdot\text{g}^{-1}$  at 0.1C-rate during the 30 cycles. The average discharge capacity was approximately  $158\text{ mAh}\cdot\text{g}^{-1}$  with a fading rate of  $-0.23\%/\text{cycle}$  at 0.1C rate during the cycling test. In addition, it was found that the average current efficiency of the LFMP/C + 2% NP-GNS + 2% HCS composite at 0.1C was approximately 98.55% during the 30-cycle test. These results indicated that all LFMP/C sample and the LFMP/C + 2% NP-GNS + 2% HCS composite exhibit excellent and stable electrochemical cycling properties. Figure 9B shows the cycle-life performance of the LFMP/C-650, LFMP/C-675, and LFMP/C-700 samples, and the LFMP/C + 2% NP-GNS + 2% HCS composite at charge/discharge rate of 1C/1C for 100 cycles for comparison. The discharge capacity of the LFMP/C-650 sample was maintained at  $122\text{--}114\text{ mAh}\cdot\text{g}^{-1}$  at 1C/1C rate during the 100-cycle test, and the average discharge capacity was approximately  $118.2\text{ mAh}\cdot\text{g}^{-1}$ , demonstrating high cycle stability with no apparent capacity decay after the 100-cycle test. It also observed that the average current efficiency of the LFMP/C-650 sample was approximately over 99%. Moreover, the discharge capacity of the LFMP/C-675 sample was kept at  $130\text{--}107\text{ mAh}\cdot\text{g}^{-1}$  at a 1C discharge rate during the 100-cycle test. Additionally, the average discharge capacity of the LFMP/C-700 was around  $115.7\text{ mAh}\cdot\text{g}^{-1}$  during the 100-cycle test and the average current efficiency of this sample was approximately 97%–98%. Particularly, the discharge capacity of the LFMP/C + 2% NP-GNS + 2% HCS composite was achieved at  $141\text{--}130\text{ mAh}\cdot\text{g}^{-1}$  at a 1C discharge rate and the average discharge capacity was around  $138\text{ mAh}\cdot\text{g}^{-1}$  during the 100-cycle test. It was found that the average current efficiency of this LFMP/C + 2% NP-GNS + 2% HCS composite was approximately 99%. These results clearly demonstrate that the

LFMP/C + 2% NP-GNS + 2% HCS composite exhibits excellent and stable electrochemical cycling properties. This may be due to the composite with good electrical conducting channels being built on the electrode material by using 2D graphene and 3D carbon sphere additives. The polarization (the charge transfer resistance) of the LFMP/C + 2% NP-GNS + 2% HCS composite was markedly reduced.

The AC impedance spectroscopy was applied to investigate the interface properties of the LFMP/C samples. The AC spectrum of the LFMP/C samples and the LFMP/C + 2% NP-GNS + 2% HCS composite is illustrated in Figure 10. The equivalent circuit for LFMP/C is displayed in inset of Figure 10. Each AC plot comprised of one semicircle at a higher frequency followed by a linear portion at a lower frequency. The lower frequency region of the straight line was considered as the Warburg impedance, which was used for long-range lithium-ion diffusion in the bulk phase.  $R_b$  indicates the bulk resistance at the electrolyte,  $R_{ct}$  refers to the charge transfer resistance at the active material interface, and CPE represents the double-layer capacitance and surface film capacitances. Table 4 summarizes the values of the  $R_b$  and  $R_{ct}$  for all LFMP/C samples. The  $R_b$  and  $R_{ct}$  values of the LFMP/C-650 sample were approximately 5.46  $\Omega$  and 156  $\Omega$ , respectively. The  $R_b$  and  $R_{ct}$  values of the LFMP/C-675 sample were approximately 4.36  $\Omega$  and 234  $\Omega$ , respectively. Moreover, the  $R_b$  and  $R_{ct}$  values of the LFMP/C-700 sample were approximately 6.06  $\Omega$  and 193.6  $\Omega$ , respectively. By contrast, the LFMP/C + 2% NP-GNS + 2% HCS composite show 5.3  $\Omega$  and 63.95  $\Omega$  for the  $R_b$  and  $R_{ct}$  values. In fact, the LFMP/C + 2% NP-GNS + 2% HCS composite showed the lowest charge transfer resistance, as compared with other LFMP/C samples. We prepared the LFMP/C composite material with 2D and 3D carbon additives, and they can build up the electrical conducting channels within LFMP electrode, which facilitate the electron transport and also greatly reduce the electrode polarization. In conclusion, the LFMP/C + 2% NP-GNS + 2% HCS composite can be prepared by a simple one-pot solid-state ball-milled process. The LFMP/C + 2% NP-GNS + 2% HCS composite showed excellent electrochemical performance; this is due to the reduction of the charge transfer resistance.

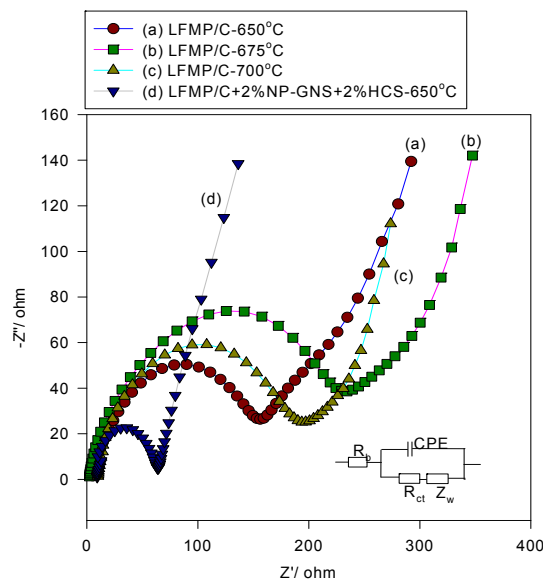


**Figure 10.** The Nyquist plots of all LFMP/C samples at open circuit potential (OCP); the inset for equivalent circuit.

**Table 4.** The parameters of alternating current (AC) impedance analysis.

Sample	$R_b$ ( $\Omega$ )	$R_{ct}$ ( $\Omega$ )
LFMP/C-650	5.46	156.24
LFMP/C-675	4.36	234.36
LFMP/C-700	6.06	193.66
LFMP/C + 2% NP-GNS + 2% HCS-650	<b>5.30</b>	<b>63.95</b>

#### 4. Conclusions

In this work, a LFMP/C material was first prepared using a wet ball-milling solid-state method. A LFMP/C + 2% NP-GNS + 2% HCS composite with mixed carbon conductors was then prepared and examined. The properties of the resulting samples were examined using XRD, SEM, TEM, micro-Raman spectroscopy, and the AC impedance spectroscopy, and galvanostatic charge-discharge methods. The LFMP/C + 2% NP-GNS + 2% HCS composite exhibited discharge capacities of 154.7, 150.3, 148.8, 136.7, 130.3, and  $120.0 \text{ mAh} \cdot \text{g}^{-1}$  at charge/discharge rates of 0.2C/0.2C, 0.2C/0.5C, 0.2C/1C, 0.2C/3C, 0.2C/5C, and 0.2C/10C, respectively. These results indicate that the LFMP/C + 2% NP-GNS + 2% HCS composite exhibited excellent high-rate capability and reliable cycle-life stability. This work demonstrated that the excellent performance of the LFMP/C can be synthesized by a one-pot solid-state method when the suitable amount of carbon conducting additives (optimum around 4 wt%) was added. Those carbon conductors play a key role in improving electrochemical performance. This study shows that the LFMP/C composite material is a good candidate for application in high-power Li-ion batteries.

**Acknowledgments:** Financial support from the Ministry of Science and Technology, Taiwan (Project No: MOST 103-2632-E-131 -001) is gratefully acknowledged.

**Author Contributions:** Chun-Chen Yang and Shinhjiang Jessie Lue wrote the paper, Yen-Wei Hung designed the experiment and did the electrochemical performance analysis. All authors examined and approved the final manuscript.

**Conflicts of Interest:** The authors declare no conflict of interest.

#### References

- Padhi, A.K.; Najundaswamy, K.S.; Goodenough, J.B. The root cause of the rate performance improvement after metal doping: A case study of LiFePO<sub>4</sub>. *J. Electrochem. Soc.* **1997**, *144*, 1188–1194. [[CrossRef](#)]
- Oh, S.; Myung, S.; Park, J.; Scrosati, B.; Amine, K.; Sun, Y. Double-structured LiMn<sub>0.85</sub>Fe<sub>0.15</sub>PO<sub>4</sub> coordinated with LiFePO<sub>4</sub> for rechargeable lithium batteries. *Angew. Chem.* **2012**, *51*, 1853–1856. [[CrossRef](#)] [[PubMed](#)]
- Oh, S.; Jung, H.; Yoon, C.; Myung, S.; Chen, Z.; Amine, K.; Sun, Y. Enhanced electrochemical performance of carbon-LiMn<sub>1-x</sub>Fe<sub>x</sub>PO<sub>4</sub> nanocomposite cathode for lithium-ion batteries. *J. Power Sources* **2011**, *196*, 6924–6928. [[CrossRef](#)]
- Osorio-Guillén, J.; Holm, B.; Ahuja, R.; Johansson, B. A theoretical study of olivine LiMPO<sub>4</sub> cathodes. *Solid State Ion.* **2004**, *167*, 221–227. [[CrossRef](#)]
- Yao, J.; Bewlay, S.; Konstantinov, K.; Drozd, V.; Liu, R.; Wang, X.; Liu, H.; Wang, G. Characterisation of olivine-type LiMn<sub>1-x</sub>Fe<sub>x</sub>PO<sub>4</sub> cathode materials. *J. Alloys Compd.* **2006**, *425*, 362–366. [[CrossRef](#)]
- Mi, C.H.; Zhang, X.G.; Zhao, X.B.; Li, H.L. Synthesis and performance of LiMn<sub>0.6</sub>Fe<sub>0.4</sub>PO<sub>4</sub>/nano-carbon webs composite cathode. *Mater. Sci. Eng. B* **2006**, *129*, 8–13. [[CrossRef](#)]
- Burba, C.; Frech, R. Local structure in the Li-ion battery cathode material Li<sub>x</sub>(Mn<sub>y</sub>Fe<sub>1-y</sub>)PO<sub>4</sub> for  $0 < x \leq 1$  and  $y = 0.0, 0.5$  and  $1.0$ . *J. Power Sources* **2007**, *172*, 870–876.
- Shin, Y.; Kim, J.; Cheruvally, G.; Ahn, J.; Kim, K. Li(Mn<sub>0.4</sub>Fe<sub>0.6</sub>)PO<sub>4</sub> cathode active material: Synthesis and electrochemical performance evaluation. *J. Phys. Chem. Solids* **2008**, *69*, 1253–1256. [[CrossRef](#)]
- Zaghbi, K.; Mauger, A.; Gendron, F.; Massot, M.; Julien, C. Insertion properties of LiFe<sub>0.5</sub>Mn<sub>0.5</sub>PO<sub>4</sub> electrode materials for Li-ion batteries. *Ionics* **2008**, *14*, 371–376. [[CrossRef](#)]
- Chen, Y.C.; Chen, J.M.; Hsu, C.H.; Yeh, J.W.; Shih, H.C.; Chang, Y.S.; Sheu, H.S. Structure studies on LiMn<sub>0.25</sub>Fe<sub>0.75</sub>PO<sub>4</sub> by *in-situ* synchrotron X-ray diffraction analysis. *J. Power Sources* **2009**, *189*, 790–793. [[CrossRef](#)]
- Baek, D.H.; Kim, J.K.; Shin, Y.J.; Chauhan, G.S.; Ahn, J.H.; Kim, K.W. Effect of firing temperature on the electrochemical performance of LiMn<sub>0.4</sub>Fe<sub>0.6</sub>PO<sub>4</sub>/C materials prepared by mechanical activation. *J. Power Sources* **2009**, *189*, 59–65. [[CrossRef](#)]
- Kim, J.; Chauhan, G.; Ahn, J.; Ahn, H. Effect of synthetic conditions on the electrochemical properties of LiMn<sub>0.4</sub>Fe<sub>0.6</sub>PO<sub>4</sub>/C synthesized by sol-gel technique. *J. Power Sources* **2009**, *189*, 391–396. [[CrossRef](#)]

13. Chen, Y.C.; Chen, J.M.; Hsu, C.H.; Lee, J.F.; Yeh, J.W.; Shih, H.C. *In-situ* synchrotron X-ray absorption studies of LiMn<sub>0.25</sub>Fe<sub>0.75</sub>PO<sub>4</sub> as a cathode material for lithium ion batteries. *Solid State Ion.* **2009**, *180*, 1215–1219. [[CrossRef](#)]
14. Martha, S.K.; Grinblat, J.; Haik, O.; Zinigrad, E.; Drezen, T.; Miners, J.H.; Exnar, I.; Kay, A.; Markovsky, B.; Aurbach, D. LiMn<sub>0.8</sub>Fe<sub>0.2</sub>PO<sub>4</sub>: An advanced cathode material for rechargeable lithium batteries. *Angew. Chem. Int. Ed.* **2009**, *48*, 8559–8563. [[CrossRef](#)] [[PubMed](#)]
15. Zou, Q.Q.; Zhu, G.N.; Xia, Y.Y. Preparation of carbon-coated LiFe<sub>0.2</sub>Mn<sub>0.8</sub>PO<sub>4</sub> cathode material and its application in a novel battery with Li<sub>4</sub>Ti<sub>5</sub>O<sub>12</sub> anode. *J. Power Sources* **2012**, *206*, 222–229. [[CrossRef](#)]
16. Liu, T.; Wu, B.; Wu, X. Realizing Fe substitution through diffusion in preparing LiMn<sub>1-x</sub>Fe<sub>x</sub>PO<sub>4</sub>-C cathode materials from MnPO<sub>4</sub>·H<sub>2</sub>O. *Solid State Ion.* **2014**, *254*, 72–77. [[CrossRef](#)]
17. Mi, Y.Y.; Gao, P.; Liu, W.; Zhang, W.; Zhou, H. Carbon nanotube-loaded mesoporous LiFe<sub>0.6</sub>Mn<sub>0.4</sub>PO<sub>4</sub>/C microspheres as high performance cathodes for lithium-ion batteries. *J. Power Sources* **2014**, *267*, 459–468. [[CrossRef](#)]
18. Hu, L.; Qiu, B.; Xia, Y.; Qin, Z.; Qin, L.; Zhou, X.; Liu, Z. Solvothermal synthesis of Fe-doping LiMnPO<sub>4</sub> nanomaterials for Li-ion batteries. *J. Power Sources* **2014**, *248*, 246–252. [[CrossRef](#)]
19. Zhong, Y.J.; Li, J.T.; Wu, Z.G.; Guo, X.D.; Zhong, B.H.; Sun, S.G. LiMn<sub>0.5</sub>Fe<sub>0.5</sub>PO<sub>4</sub> solid solution materials synthesized by rheological phase reaction and their excellent electrochemical performances as cathode of lithium ion battery. *J. Power Sources* **2013**, *234*, 217–222. [[CrossRef](#)]
20. Scosati, B.; Garche, J. Lithium batteries: Status, prospects and future. *J. Power Sources* **2010**, *195*, 2419–2430. [[CrossRef](#)]
21. Goriparti, S.; Miele, E.; Angelis, F.D.; Fabrizio, E.D.; Zaccaria, R.P.; Capiglia, C. Review on recent progress of nanostructured anode materials for Li-ion batteries. *J. Power Sources* **2014**, *257*, 421–443. [[CrossRef](#)]
22. Zhao, W.; Liu, Y.; Zhang, X. Preparation and characterization of hollow Co<sub>3</sub>O<sub>4</sub> spheres. *Mater. Lett.* **2008**, *62*, 772–774. [[CrossRef](#)]
23. Zhang, J.; Guo, B.; Yang, Y.; Shen, W.; Wang, Y.; Zhou, X.; Wu, H.; Guo, S. Gas molecule adsorption in carbon nanotubes and nanotube bundles. *Carbon* **2015**, *84*, 467–478.
24. Yang, C.C.; Chen, Y.C.; Liao, Y.C. Comparison of electrochemical performances of LiFePO<sub>4</sub>/C composite materials by two preparation routes. *Mater. Res. Bull.* **2012**, *47*, 2622–2626. [[CrossRef](#)]



© 2016 by the authors; licensee MDPI, Basel, Switzerland. This article is an open access article distributed under the terms and conditions of the Creative Commons Attribution (CC-BY) license (<http://creativecommons.org/licenses/by/4.0/>).